Simple phase extraction in x-ray differential phase contrast imaging*

Xin Liu(刘鑫)†, Jin-Chuan Guo(郭金川), Yao-Hu Lei(雷耀虎), Ji Li(李冀), and Han-Ben Niu(牛憨笨)

Key Laboratory of Optoelectronic Devices and Systems of Ministry of Education and Guangdong Province, College of Optoelectronic Engineering, Shenzhen University, Shenzhen 518060, *China*

(Received 14 September 2015; revised manuscript received 12 October 2015; published online 10 January 2016)

A fast and simple method to extract phase-contrast images from interferograms is proposed, and its effectiveness is demonstrated through simulation and experiment. For x-ray differential phase contrast imaging, a strong attenuation signal acts as an overwhelming background intensity that obscures the weak phase signal so that no obvious phase-gradient information is detectable in the raw image. By subtracting one interferogram from another, chosen at particular intervals, the phase signal can be isolated and magnified.

Keywords: x-ray imaging, x-ray interferometry, Talbot and self-imaging effects, phase contrast imaging

PACS: 87.59.–e, 07.60.Ly, 42.30.Rx, 87.57.–s **DOI:** 10.1088/1674-1056/25/2/028704

1. Introduction

X-ray phase-sensitive technique is an important extension of x-ray radiographic imaging that is widely used in medicine, nondestructive testing, and security. Besides conventional absorption images, phase-sensitive imaging can offer two other images: phase distribution and dark field distribution.[1–4] Various phase-sensitive techniques have been proposed and developed over the past decade.[5–21] Among them, the differential phase contrast (DPC) imaging can be used in a broad range of applications due to its low requirements for source coherence, mechanical stability and detector resolution.[6]

Without specimen, interferograms of phase gratings consist of many regular fringes. An object introduced in the light path distorts the fringes, and the resulting variations in the intensity pattern encode the wavefront phase. The obtaining of the phase distribution of the sample requires a phase retrieval procedure that calculates the phase image from multiple intensity measurements. In the visible light region, Fourier-transform and phase-stepping algorithms are common phase retrieval methods.[8,9] Naturally, those techniques were introduced in DPC imaging system and yielded excellent results[8,10,11] No less than three images are needed for a phase-stepping algorithm; usually, the number of intensity measurements is in a range of $5 \sim 11$.[12] Multiple exposures cause excess exposure time and increased x-ray absorption, which are disadvantageous in medical and biological applications. Bennett *et al.* proposed a fast and simple algorithm that requires no movement of the grating.[10] However, it requires individual harmonic spectrum, resulting in the loss of high spatial frequency.

In this paper, we deduce the intensity distribution in a detecting plane for a finite-size x-ray source. The formula of intensity shows that the analysis grating parameters and x-ray source spatial coherence have the greatest effects on phase signals. The attenuation signals have more contributions than the phase shift signals in intensity image. Thus, usable phase information requires a map of phase retrieval. We propose a fast and simple method based on the intensity formula to extract the phase-gradient signals from the raw data without losing the high spatial frequency. Relative numerical calculations and experimental results demonstrate our method effectiveness.

2. Theoretical background

We consider a common x-ray interferometer with a finite-size x-ray source as shown in Fig. 1, where R and l denote the distances between the source grating (G_0) and phase grating (G_1), which is downstream of the sample, and between G_1 and the analysis grating (G_2), respectively. First, we consider only a monochromatic point x-ray source of wavelength λ, then we extend the result to a multi-slit x-ray source.

2.1. Spherical wave source

The complex transmission function $T(x)$ of G_1 can be expressed with a Fourier series as

$$T(x) = \sum_{n=-\infty}^{\infty} a_n \exp\left(\mathrm{i}n\frac{2\pi}{p_1}x\right), \tag{1}$$

where a_n is the amplitude of the n-th harmonic and p_1 is the period of the grating. At a distance l downstream of G_1, the complex amplitude of the propagating field is given by

$$U(x,l) = \exp\left[\mathrm{i}\pi\frac{x^2}{\lambda}\left(\frac{1}{l}-\frac{1}{Ml}\right)\right]$$

*Project supported by the National Natural Science Foundation of China (Grant Nos. 61101175, 61571305, and 61227802).

†Corresponding author. E-mail: sblx@szu.edu.cn

© 2016 Chinese Physical Society and IOP Publishing Ltd

$$\times \sum_{n=-\infty}^{\infty} a_n \exp\left(-\mathrm{i}\pi n^2 \frac{l\lambda}{Mp_1^2}\right) \exp\left(2\pi \mathrm{i} \frac{n}{Mp_1} x\right), \quad (2)$$

by using the paraxial approximation and a spherical beam illumination of G_1, where λ is the x-ray wavelength and $M = (R+l)/R$ is the magnification. For $R \gg l$, $M \approx 1$; hence, the phase factor of Eq. (2) is negligible. Then

$$U(x,l) \approx \sum_{n=-\infty}^{\infty} a_n \exp\left(-\mathrm{i}\pi n^2 \frac{l\lambda}{Mp_1^2}\right) \exp\left(2\pi \mathrm{i} \frac{n}{Mp_1} x\right). \quad (3)$$

When a sample is placed just before G_1, G_1 will split the incident light carrying the complex amplitude of the sample into different diffraction orders. As a consequence, the amplitude transmission function of the sample $A(x,y)\mathrm{e}^{\mathrm{i}\phi(x,y)}$ is shifted by ns along the x-axis, such that

$$U(x,y;l) = \sum_{n=-\infty}^{\infty} a_n \exp\left(-\mathrm{i}\pi n^2 \frac{l\lambda}{Mp_1^2}\right) \exp\left(2\pi \mathrm{i} \frac{n}{Mp_1} x\right) \times A\left(\frac{x-ns}{M}, \frac{y}{M}\right) \exp\left[\mathrm{i}\phi\left(\frac{x-ns}{M}, \frac{y}{M}\right)\right], \quad (4)$$

where the shearing amount is $s = l\lambda/p_1$. Therefore, from Eq. (4), the intensity $I(x,y;l) = U(x,y;l)U^*(x,y;l)$ is given by

$$I(x,y;l) = \sum_{m,n} a_n a_m^* \exp\left[-\mathrm{i}\pi(n^2-m^2)\frac{l\lambda}{Mp_1^2}\right] \times A_n A_m \exp[p(x)], \quad (5)$$

where the superscript "$*$" denotes the conjugate, and

$$p(x) = 2\pi \mathrm{i} \frac{n-m}{Mp_1} x + \mathrm{i}\left[\phi\left(\frac{x-ns}{M}, \frac{y}{M}\right) - \phi\left(\frac{x-ms}{M}, \frac{y}{M}\right)\right], \quad (6)$$

$$A_n = A\left(\frac{x-ns}{M}, \frac{y}{M}\right), \quad A_m = A\left(\frac{x-ms}{M}, \frac{y}{M}\right). \quad (7)$$

Assuming that the shearing amount ns is sufficiently small,[5] equations (5) and (7) respectively become

$$p(x) \approx 2\pi \mathrm{i} \frac{n-m}{Mp_1}\left[x - l\frac{\lambda}{2\pi}\frac{\partial\phi}{\partial x}\right], \quad (8)$$

$$A_n\left(\frac{x-ns}{M}, \frac{y}{M}\right) \approx A_m\left(\frac{x-ms}{M}, \frac{y}{M}\right) \approx A\left(\frac{x}{M}, \frac{y}{M}\right). \quad (9)$$

2.2. Multi-slit x-ray source

According to the van Cittert–Zernike theorem, the intensity distribution of a source will smoothen the interferogram $I(x,y;l)$, so in the detecting plane, the intensity $I'(x,y;l)$ is calculated as[15]

$$I'(x,y;l) = I_s\left(\frac{x}{l/R}, \frac{y}{l/R}\right) \otimes I(x,y), \quad (10)$$

where $I_s(x,y)$ denotes the source intensity, which is the convolution of rectangle function $\mathrm{rect}(x/a)$ with a sum of delta functions,

$$I_s(x) = \mathrm{rect}\left(\frac{x}{a}\right) \otimes \sum_{n=-N}^{N} \delta(x - np_0). \quad (11)$$

The multi-slit source has periodicity p_0 and the slit width α, as illustrated in Fig. 1.

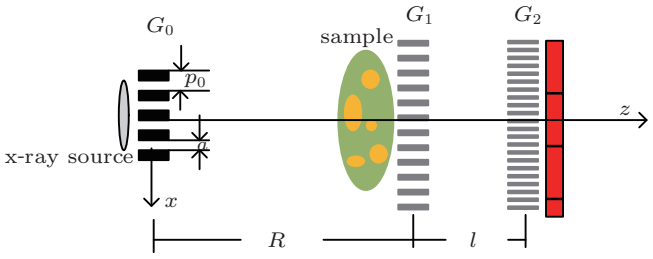


Fig. 1. (color online) X-ray differential phase contrast imaging and coordinate system.

2.3. Intensity distribution

The final intensity distribution on the detector is determined by taking into account the effect of the third grating G_2 with periodicity p_2. Assuming that G_1 and G_2 are parallel, the intensity signal detected by one pixel, according to the model in Fig. 2, is

$$I'' = \int_{\chi}^{\chi+D} I'(x,y)\,\mathrm{d}x + \int_{p_2+\chi}^{p_2+\chi+D} I'(x,y)\,\mathrm{d}x + \cdots + \int_{(k-1)p_2+\chi}^{(k-1)p_2+\chi+D} I'(x,y)\mathrm{d}x, \quad (12)$$

where the relative position between x-ray fringes and G_2 is χ, G_2 has 100% absorption efficiency, the aperture width of one periodicity is D, and one pixel can collect k periodicities of x-ray fringes.

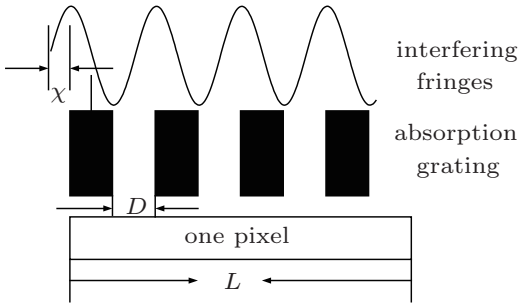


Fig. 2. Detection model of x-ray interfering fringes.

The signal I'' would be a very complex expression if we implement Eq. (4), (10), and (11) into Eq. (12) without any approximations. Using the special structure of G_1 at the Talbot distance, we can obtain a compact expression of I''. For example, when the duty cycle of G_1 is 0.5 and the imaging distance of G_1 satisfies

$$l = M\frac{\lambda}{8p_1^2}, \quad (13)$$

and the intensity signal $I(x,y;l)$ in Eq. (5) is given by

$$I(x,y;l) = \frac{A^2(x/M,y/M)(1-\cos\theta)}{\pi^2} \times \left[\frac{19}{9}+\cos\left(\frac{2\pi}{p_2}\left(x-l\frac{\lambda}{2\pi}\frac{\partial\phi}{\partial x}(x/M,y/M)\right)\right)\right], \quad (14)$$

where only the 0, ±1 diffraction orders are considered, θ denotes the phase shift of G_1, and $p_2 = Mp_1/2$. We assume that $A(x,y)\,\mathrm{e}^{\mathrm{i}\phi(x,y)}$ varies slowly with x, so the effect of convolving $A(x,y)$ with $\phi(x,y)$ in Eq. (10) can be neglected.[15] That is to say, we neglect the scatting contribution to the intensity distribution $I(x,y;l)$. The same assumption in Eq. (12) results in the integral

$$I''(x,y) = \Gamma(x/M,y/M)\left[\frac{19}{9}+\gamma\cos\left[\phi(x/M,y/M)+\alpha\right]\right], \quad (15)$$

where

$$\Gamma(x,y) = kD(2N+1)\frac{aD}{p_0p_2}\frac{8lp_2^2}{\pi^2R}A^2(x,y)(1-\cos\theta),$$
$$\alpha = \frac{2\pi}{p_2}\left(x+\frac{D}{2}\right),$$
$$\varphi(x,y) = -l\frac{\lambda}{p_2}\frac{\partial\phi}{\partial x}(x,y),$$
$$\gamma = \mathrm{sinc}\frac{a}{p_0}\,\mathrm{sinc}\frac{D}{p_2},$$

and $\mathrm{sinc}\,x = \sin\pi x/\pi x$. At the same time, G_1 is located at special positon such that

$$\frac{p_0}{R} = \frac{p_2}{l}. \quad (16)$$

Now we can discuss the contributions of $A(x,y)$ and $\phi(x,y)$ to the intensity signal $I''(x,y)$. The value of γ determines the contribution of $A(x,y)$ and small apertures of G_0 and G_2 can increase the occupancy rate of $\phi(x,y)$ in $I''(x,y)$. However, a and D cannot be very small. In general, we choose parameters such that half the incident light passes though G_0 and G_2, which means that $a/p_0 = D/p_2 = 0.5$ and $\gamma \approx 0.4$. Thus, the phase information amplitude only contributes 15% of the measured intensity, and most energy is attributed to the attenuation term $\Gamma(x,y)$. The phase contrast signals, which provide more structural information, are consequently hard to detect for the attenuation signal.

3. Method

We estimate the values of $\phi(x,y)$ and $A^2(x,y)$ from the following equations:

$$\phi = \frac{2\pi}{\lambda}\int\delta(x,y,z)\,\mathrm{d}z, \quad (17)$$

$$A^2(x,y) = \exp\left(-\int\mu(x,y,z)\,\mathrm{d}z\right), \quad (18)$$

where δ is the real part of the complex refractive index and μ is the quality factor of the attenuation. For light material, δ is typically on the order of 10^{-6}–10^{-7} for 20 keV–30 keV x-rays, so that $\phi(x,y)$ is usually quite small(a few arc seconds), except is areas near edges and boundaries. We assume again that $\phi(x,y)$ varies slowly varying spatially and is sufficiently small so that equation (13) can be expanded and approximated as[15]

$$I''(x,y) \approx \Gamma(x,y)\left[19/9+\gamma\cos\alpha-\gamma\phi(x,y)\sin\alpha\right]. \quad (19)$$

If the strong background signal $\Gamma(x,y)$ can be eliminated from Eq. (19), the image intensity would be proportional to $\phi(x,y)$. A simple approach can delete this background signal by using only two raw images. A first interferogram I_1'' is collected with the phase grating at α, and a second I_2'' is obtained by moving the phase grating to $\alpha+\pi$. Subtracting I_1'' from I_2'' results in

$$I'''(x,y) = \frac{I_2''(x,y)-I_1''(x,y)}{I_2''(x,y)+I_1''(x,y)} = 2k_1\phi(x,y)+k_2, \quad (20)$$

where k_1 and k_2 are constants that do not affect image contrast. Since $\phi(x,y)$ of an object is generally a spatially random distribution, we can reasonably expect

$$\langle 2k_1\phi(x,y)+k_2\rangle = k_2, \quad (21)$$

where $\langle\cdot\rangle$ indicates the average over the entire intensity image. Thus, the k_2 can be estimated and removed from the I''. On the boundaries, due to the large gradient, equation (20) can be rewritten as

$$I_3 = 2\cos[\alpha+\phi(x,y)], \quad (22)$$

which means that the signal intensity is not equal to the gradient of the phase. Nevertheless, since all edges are described by the same expression, I''' can still give structural information. Our simple method removes the background signals and isolates phase signals.

4. Simulation and experiment

4.1. Numerical calculation

In this section, we show the results of numerical calculations of one carbon ball on the basis of Eqs. (4), (10), and (12).

Figures 3(a) and 3(b) are the raw images with the G_1 placed at different positions, and figures 3(c) and 3(d) are the intensity profiles along the red bars, respectively. The following parameters are used in this simulation: $\lambda = 0.041$ nm, 1-mm carbon ball diameter, $\delta = 5.2\times10^{-6}$, $\mu = 0.584$ cm^{-1},

$p_1 = 5.6$ μm, $l = 105$ mm, $R = 1470$ mm, $p_0 = 42$ μm, $p_2 = 3$ μm, and 27-μm pixels. Except in the line profiles in Figs. 3(c) and 3(d), it is hard to find the gradient signal of phase. Using Eq. (20), we obtain the image of phase gradient image shown in Fig. 4.

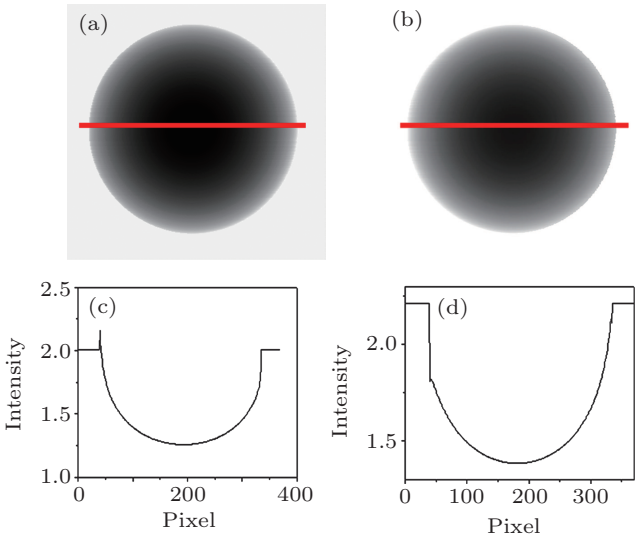


Fig. 3. (color online) Raw intensity measurements of a carbon ball. The positions of G_1 are α and $\alpha + \pi$ in panels (a) and (b), respectively. The line profiles in panels (a) and (b) correspond to the red lines in panels (a) and (b), respectively.

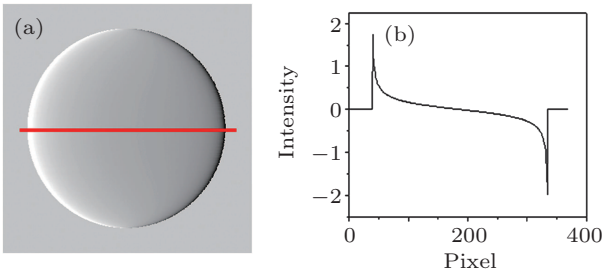


Fig. 4. (color online) (a) Phase-gradient image and (b) line profile corresponding to red line in panel (a).

4.2. Experiments

A fresh pig foot purchased from a supermarket was imaged using a non-absorption grating imaging system described in Ref. [14]. Two raw data images and a phase gradient image are shown in Figs. 5 and 6(a), respectively. It is difficult to visually distinguish the two raw images in Figs. 5(a) and 5(b). However, the phase gradient intensity profile of Fig. 6(b) shows the fine distinction caused by the phase shift. After removing the attenuation information using our method, the phase-gradient is detectable in the intensity distribution (Fig. 6(a)).

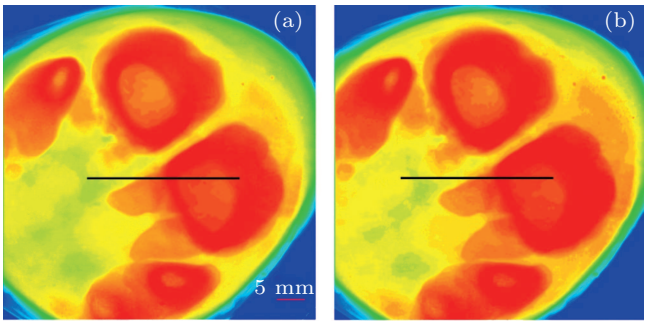


Fig. 5. (color online) Radiography images: panels (a) and (b) are raw images collected with the phase grating at two different positions.

The x-ray source is a common x-ray tube with no filter, at a 70-kV acceleration voltage, and with a 2-mA anode current. The distance between sample and detector is 105 mm. The phase grating is made of silicon, has a 5.6-μm period, a 0.5-duty ratio, and a 40-μm depth, corresponding to a π phase shift for 31-keV x-rays. The scintillator is directly coupled with an ANDOR 2048×2048-pixel (13.5 μm/pixel) CCD camera through a fiber optical tape, with 2× demagnification.

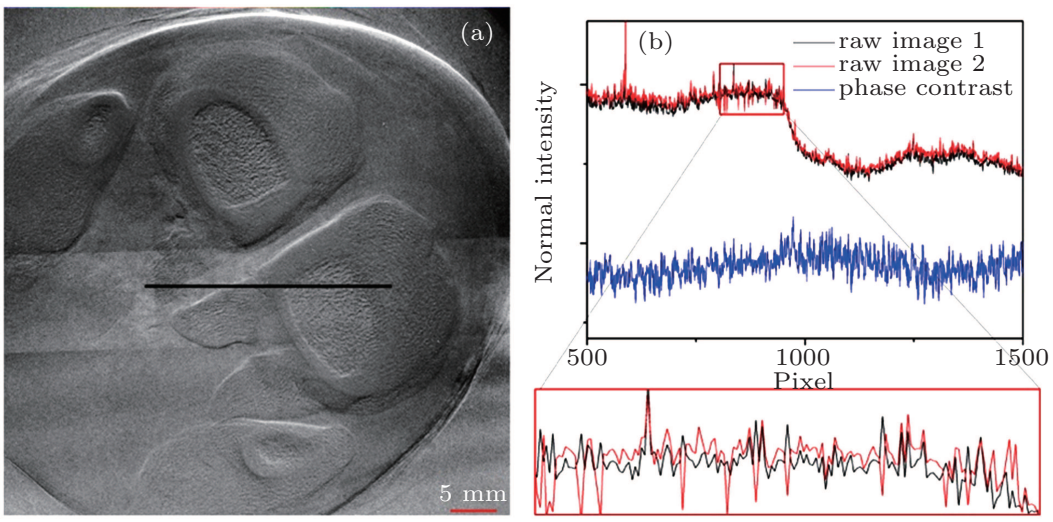


Fig. 6. (color online) (a) Phase-gredient images calculated from the raw images of Fig. 5. The structures of trabeculae clearly emerge in the phase contrast, while they are invisible in Fig. 5. (b) Intensity profiles along the black lines in Figs. 5(a), 5(b), and 6(a). The curve at the bottom is a detailed part of the profile. Figures 5(a), 5(b), and 6(a) have the same scale bar.

5. Conclusions

We present intensity formulae for x-ray Talbot interferometry with a partial spatial coherent source. On the basis of these formulae, we find that the structural parameters of the source and analyzer gratings greatly affect the phase-gradient signal intensity. For G_0 and G_2, a larger aperture in one periodicity dramatically reduces the amplitude of phase information to the extent that the phase-gradient image is difficult to detect in raw data. We propose a simple approach to extracting the phase image from raw signals and demonstrate its effectiveness through numeral calculation and experiment. Compared with the existing stepping methods using no less than three interferograms, our method is simpler and much faster.

References

[1] Momose A, Takeda T, Itai Y and Hirano K 1996 *Nat. Med.* **2** 473
[2] Davis T J, Gao D, Gureyev T E, Stevenson A W and Wilkins S W 1995 *Nature* **373** 595
[3] Wilkins S W, Gureyev T E, Gao D, Pogany A and Stevenson W 1996 *Nature* **384** 335
[4] Wang S H, Margie P O, Momose A, Han H J, Hu R F, Wang Z L, Gao K, Zhang K, Zhu P P and Wu Z Y 2015 *Chin. Phys. B* **24** 068703
[5] Momose A, Kawamoto S, Koyama I, Hamaishi Y, Takai K and Suzuki Y 2003 *Jpn. J. Appl. Phys.* **42** L866
[6] Weitkamp T, Diaz A, David C, Pfeiffer F, Stampanoni M, Cloetens P, and Ziegler E 2005 *Opt. Express* **13**
[7] Revol V, Kottler C, Kaufmann R, Straumann U and Urban C 2010 *Rev. Sci. Instrum.* **81** 073709
[8] Takeda M, Ina H and Kobayashi S 1982 *J. Opt. Soc. Am.* **72** 156
[9] Schofield M A and Zhua Y 2003 *Opt. Lett.* **28** 1194
[10] Bennett E, Kopace R, Stein F and Wen H 2010 *Med. Phys.* **37** 6047
[11] Wen H, Bennett E, Kopace R, Stein F and Pai V 2010 *Opt. Lett.* **35** 1932
[12] Pfeiffer F, Bech M, Bunk O, Kraf t P, Eikenberry E F, Bronnimann C, Grunzweig C and David C 2008 *Nat. Mater.* **7** 134
[13] Zhu P, Zhang K, Wang Z, Liu Y, Liu X, Wu Z, McDonald S A, Marone F, and Stampanoni M 2010 *Proc. Natl. Acad. Sci. USA* **107** 13576
[14] Du Y, Liu X, Lei Y H, Guo J C and Niu H B 2011 *Opt. Express* **19** 22669
[15] Yashiro W and Momose A 2015 *Opt. Express* **23** 9233
[16] Kim J, Lee S W and Cho G 2014 *Nucl. Instrum. Methods Phys. Res. Sec. A: Accelerators, Spectrometers, Detectors and Associated Equipment* **746** 26
[17] Modregger P, Rutishauser S, Meiser J, David C and Stampanoni M 2014 *Appl. Phys. Lett.* **105** 024102
[18] Peter S, Modregger P, Fix M K, Volken W, Frei D, Manserd P and Stampanoni M 2014 *J. Synchro. Rad.* **21** 613
[19] Huang J H, Du Y, Lei Y H, Liu X, Guo J C and Niu H B 2014 *Acta Phys. Sin.* **63** 168702 (in Chinese)
[20] Zhang X D, Xia C J, Xiao X H and Wang Y J 2014 *Chin. Phys. B* **23** 044501
[21] Han Y, Li L, Yan B, Xi X Q and Hu G E 2015 *Acta Phys. Sin.* **64** 058704 (in Chinese)